Evans Blue Attachment Enhances Somatostatin Receptor Subtype-2 Imaging and Radiotherapy

Rui Tian[1,2], Orit Jacobson[2*], Gang Niu[2], Dale O. Kiesewetter[2], Zhantong Wang[2], Guizhi Zhu[2], Ying Ma[2], Gang Liu[1] and Xiaoyuan Chen[2*]

1. State Key Laboratory of Molecular Vaccinology and Molecular Diagnostics & Center for Molecular Imaging and Translational Medicine, School of Public Health, Xiamen University, Xiamen 361102 China.
2. Laboratory of Molecular Imaging and Nanomedicine, National Institute of Biomedical Imaging and Bioengineering, National Institutes of Health, Bethesda, Maryland, USA.

* Corresponding authors: Orit Jacobson (orit.jacobsonweiss@nih.gov); Xiaoyuan Chen (shawn.chen@nih.gov)

Supplementary Information

General

Synthesis and characterization of DOTA-Maleimide-EB (EB) derivative was previously reported by us (1). TATE peptide containing Dde protecting group, TATE(Dde), was purchased from CSBio Company, Inc. (Menlo Park, CA). S-Tritylmercaptoacetic acid NHS ester was synthesized following the published procedure (2). DOTA-TATE was synthesized using a minor modification of the published procedure (1, 3). Analytical high-performance liquid chromatography (HPLC) used Phenomenex Luna C8 column (5 μm, 4.60×150 mm) with a gradient system starting from 95% solvent A (50mM NH_4OAc, pH 6.5) and 5% solvent B (CH_3CN) and changing to 65% solvent B at 35 min at flow rate of 1 mL/min. The ultraviolet absorbance was monitored at 254 and 600 nm. Compounds were purified on Higgins column (C-18, 5μm, 250 x 20 mm) using gradient system as described above except changes in the solvents [solvent A: 0.1% trifluoroacetic acid (TFA)/H_2O, solvent B: 0.1% TFA/CH_3CN] and flow rate of 12 mL/min. LC-MS analysis utilized analogous procedures to those reported (1).

Synthesis of thiolated TATE (TATE-SH)

TATE(Dde) (1 eq.) was dissolved in 1 mL dimethylformamide (DMF). Then S-Tritylmercaptoacetic acid NHS ester (1.1 eq.) was added, followed by addition of 5 eq. of diisopropylethylamine (DIPEA). The reaction was mixed for 4-5 h at room temperature until full conversion into protected TATE was observed by HPLC analysis. Then 2% (w/v) of Hydrazine was added and the reaction mixture stirred for additional 0.5 h. Lysine deprotection

was confirmed by LCMS and the crude mixture was purified using HPLC. The peptide was collected and lyophilized overnight. Deprotection of S-trityl from TATE employed TFA:H_2O: 1,2-ethanedithiol (90:5:5) at room temperature for 1 h to give TATE-SH. LC-MS analysis confirmed mass of 1119 $[M-H]^-$. The crude mixture was purified on HPLC to give TATE-SH in a chemical purity >95% and a chemical yield of 38-40%.

Synthesis of EB-TATE

TATE-SH (1 eq) was dissolved in 10% (v/v) Dimethyl sulfoxide (DMSO) and 90% of 0.1% (w/v) Na-ascorbate in PBS and mixed with 1 eq of EB derivative dissolved in 0.1% Na-ascorbate (w/v) in PBS to a total volume of 1-2 mL. The reaction was stirred for 2 h at room temperature and purified by HPLC to give EB-TATE in a chemical purity >95% and a yield of 65-70%. LC-MS analysis confirmed mass of 2328 $[M-H]^-$.

Radiochemistry

^{86}Y was purchased from University of Wisconsin and NIH Cyclotron Facility. ^{90}Y was purchased from Perkin-Elmer. 10 µL of $^{86}YCl_3$ (37 MBq) and/or $^{90}YCl_3$ (111 MBq) were diluted with 0.5 mL 0.4 M ammonium acetate pH 5.6. Then EB-TATE or DOTA-TATE (40 nmol in 10-20 µL) was added and the reaction mixed for 30 min at 37°C. Purity of the products was assayed by radio-TLC (AR-2000 Bioscan scanner), using iTLC plates (Fisher) and 0.1 M Citric acid pH 5 as the developing solvent. R_f of free $^{86/90}$Y ~ 0.9; R_f of $^{86/90}$Y-EB-TATE and TATE ~ 0.1. The compounds were labeled in radiochemical purity > 95% and specific activity ranging from 6.6-6.8 mCi/µmol for ^{86}Y-EB-TATE/TATE to 140-150 mCi/µmol for ^{90}Y-EB-TATE/TATE. Synthesis of ^{64}Cu-DOTA-TATE was done in the same manner. Synthesis of ^{68}Ga-DOTA-TATE was conducted according to the published procedure (3).

Albumin binding assay

In vitro albumin binding affinity of EB-TATE was evaluated by competitive study against ^{86}Y-EB-TATE using streptavidin agarose beads (Thermo Fisher Scientific) and biotinylated human serum albumin (Protein Mods). 200 µL of beads slurry were washed five times with PBS by centrifuge and then resuspend in PBS and mixed with 600 µL biotinylated-HSA (1 mg/mL, 3-molar excess) for 1 h at room temperature. Then the mixture was extensively washed with PBS to remove excess of biotinylated-HSA. Next, the labeled beads were incubated with radiolabeled 7.4 KBq ^{86}Y-EB-TATE and increasing concentrations (1 nM-100 µM) of unlabeled EB-TATE for 1.5 h at room temperature in a 96-well membrane plate. After the incubation, the plate was washed several times with PBS and the radioactivity bound to the

beads was measured using a gamma-counter. Each time point was measured in triplicate.

^{90}Y-EB-TATE Biodistribution

1.85 MBq of ^{90}Y-EB-TATE was intravenous injected to HCT116/SSTR2 tumor bearing mice. At days 1 (n = 5), 4 (n = 6), 7 (n = 6) and 12 (n = 7) post-injection, mice were sacrificed and tumor, heart, lung, liver, spleen, intestine, kidney, muscle, bone and blood were collected. The tissues were minced, weighed and dissolve in 1-1.5 mL of SOLVABLE (Perkin-Elmer) in 20 mL scintillation vials. The vials were heated to 50-55 °C for 3 h with agitation every 30 min and then left at room temperature for 24 h. After tissue dissolution, 200 µL of 30% H_2O_2 were added and the mixture, incubated at 50-55 °C for 1 h. After cooling, 16 mL of scintillation cocktail (ULTIMA Gold, Perkin-Elmer) were added to each vial. Radioactivity was measured by a beta counter (WinSpectral, Perkin-Elmer) and the results were calculated as percent injected dose per gram tissue (%ID/g).

***In vivo* stability**

Mice bearing HCT116/SSTR2 tumors were each injected with 1.85 MBq of ^{90}Y-EB-TATE, tumors were collected at different time points post-injection, minced, and dissolved in 50 µL of CH_3CN:CH_3OH (1:1). The slurry solution was centrifuge for 1-2 min at 10,000 rpm. An aliquot was taken and analyzed by iTLC plate, as described in the radiochemistry methodology section above.

Figure Legends

Supplementary Fig. S1. Representative immunofluorescence staining (X20) of anti-SSTR2 (green) and nucleus (DAPI, blue) in tumor tissues from HCT116/SSTR2, HCT116 and AR42J xenografts.

Supplementary Fig. S2. (A) Cell binding affinity assays of TATE *vs.* EB-TATE in AR42J cells. IC_{50} of TATE (red curve): 3.46 ± 0.88 nM, and IC_{50} of EB-TATE (blue curve): 9.16 ± 0.09 nM. Results are shown as average ± SD of triplicates. (B) Uptake and internalization of ^{86}Y-EB-TATE and ^{86}Y-TATE in AR42J (SSTR2^{+}) cells in the presence of 1% (w/v) of human serum albumin. Blocking studies were evaluated at 24 h. Results are shown as average ± SD of triplicates. ***$P < 0.001$. (C) Binding affinity assay of ^{86}Y-EB-TATE and biotinylated-albumin using streptavidin agarose beads. IC_{50} of EB-TATE 1.92 ± 0.34 μM. Results are shown as average ± SD of triplicates.

Supplementary Fig. S3. (A) Time-activity curves of ^{86}Y-EB-TATE and ^{86}Y-TATE in different organs over time, calculated from PET quantification. (B) Biodistribution of ^{86}Y-EB-TATE and ^{86}Y-TATE in HCT116/SSTR2 and HCT116 xenografts at 48 h post injection.

Supplementary Fig. S4. (A) Uptake of ^{86}Y-EB-TATE in AR42J tumor model with and without co-injection of EB-TATE excess (block) over time. Results are presented as %ID/g mean and max values. (B) Biodistribution of ^{86}Y-EB-TATE in AR42J xenografts at 48h post injection with or without unlabeled EB-TATE. *p<0.05, **$P < 0.01$, ***$P < 0.001$.

Supplementary Fig. S5. Area under the curves (AUCs) of EB-TATE (blue) and TATE (orange) calculated from the radioactivity accumulation in the tumor over time.

Supplementary Fig. S6. Representative pictures of tumor-bearing mice before radionuclide therapy (A) during the treatment when the tumor is still visible (B) and at the end of the study, at day 180 when the tumor almost disappeared (C) or completely eradicated (D). Red arrows indicate tumor location. Enlargement of the tumor region before (blue) and after (green) treatment are shown in the lower panel.

Supplementary Fig. S7. ^{68}Ga-DOTA-TATE PET imaging of HCT116/SSTR2 xenograft after radionuclide tumor therapy of (A) mice injected with saline and (B) mice injected 3.7 MBq ^{90}Y-EB-TATE, about 80 days post initial treatment when the tumor started to re-grow. Images were acquired 60 min after injection of ^{68}Ga-DOTA-TATE. White arrows indicate tumor location.

Supplementary Fig. S8. Representative immunofluorescence staining (X 20) of anti-SSTR2 (green) and nucleus (DAPI, blue) in mice bearing HCT116/SSTR2 tumor model after radionuclide tumor therapy (A) with saline and (B) with 3.7 MBq of ^{90}Y-EB-TATE that was sacrificed at day 77 after tumor partial re-growth.

Supplementary Fig. S9. Representative immunofluorescent staining (X 20) of anti-SSTR2 (green) and nucleus (DAPI, blue), 1, 7 and 14 days after injection of saline (HCT116/SSTR2 tumor model, upper panel) or 7.4 MBq of ^{90}Y-EB-TATE in HCT116 (middle panel) and HCT116/SSTR2 (lower panel) xenografts.

Supplementary Fig. S10. Body weight change of HCT116/SSTR2, HCT116 tumor bearing mice during the radiotherapy study. Red arrows indicate injection of the radiotherapeutic dose.

Supplementary Fig S11. Body weight change of AR42J tumor bearing mice during the radiotherapy study. Red arrow indicates injection of the radiotherapeutic dose.

Supplementary Fig. S12. Representative H&E staining of different organs from mice after radionuclide therapy (day 14).

Supplementary Fig. S13. Representative H&E staining of bone (A) and kidneys (B) from mice 3 to 4 months after radionuclide therapy.

Supplementary Fig. S14. Biodistribution of ^{90}Y-EB-TATE in HCT116/SSTR2 xenografts at different time points post injection (n=5-7 for each time point).

Supplementary Fig. S15. (A) Representative radioTLC analysis for ^{90}Y -EB-TATE and uncoordinated free ^{90}Y using iTLC plate and 0.1 M citric acid at pH 5 as developing solvent. (B) Representative radioTLC analysis of extracts from HCT116/SSTR2 tumors as a function of time following injection of ^{90}Y-EB-TATE.

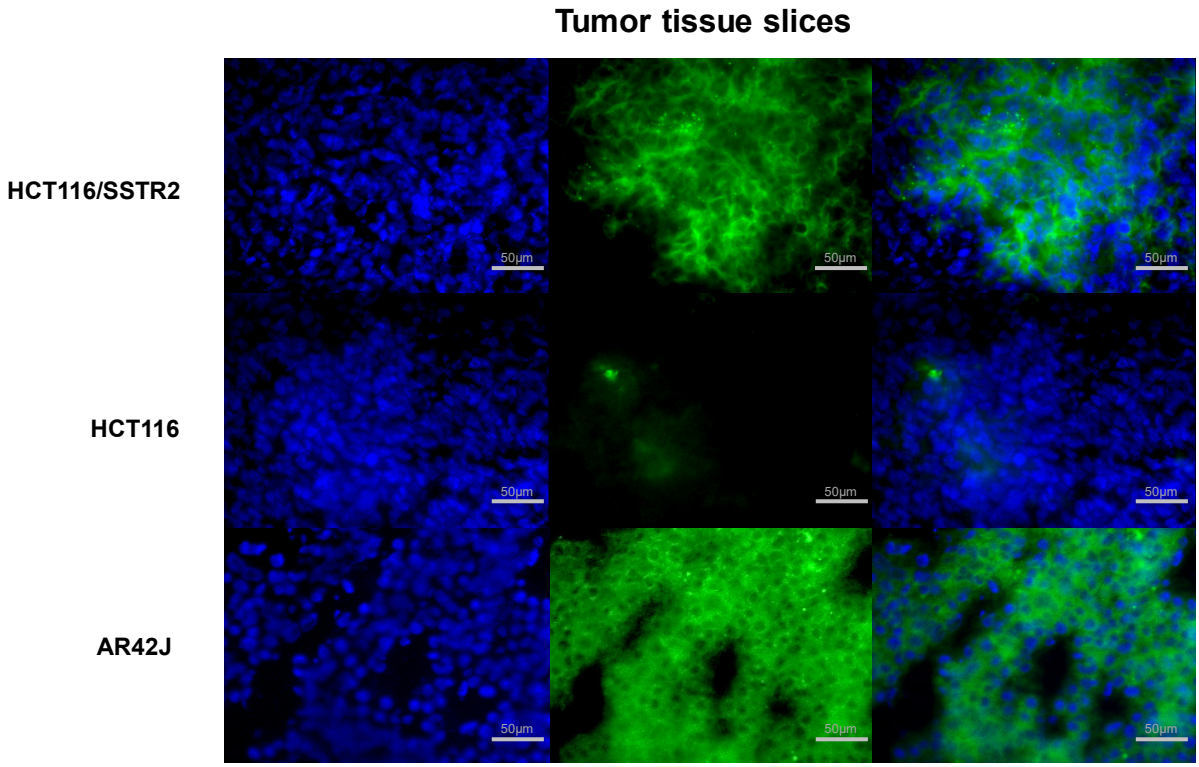

Figure S1

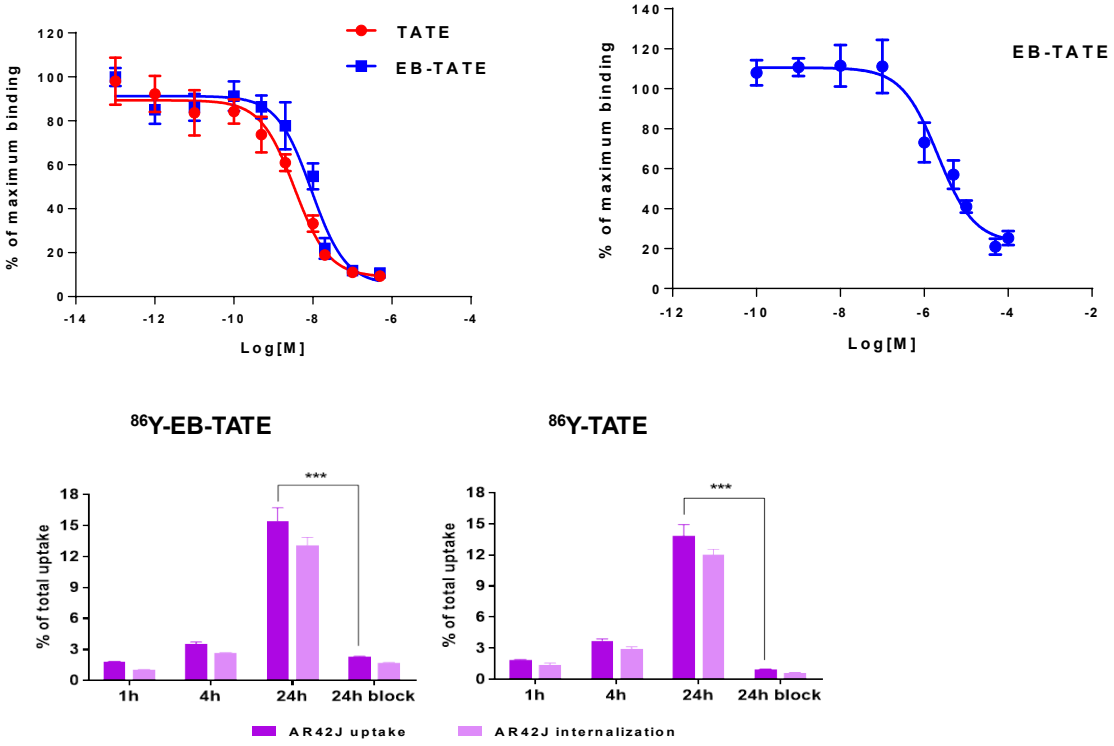
TATE
EB-TATE
% of maximum binding
Log[M]
EB-TATE
% of maximum binding
Log[M]
86Y-EB-TATE
86Y-TATE
% of total uptake
1h
4h
24h
24h block
***
AR42J uptake
AR42J internalization

Figure S2

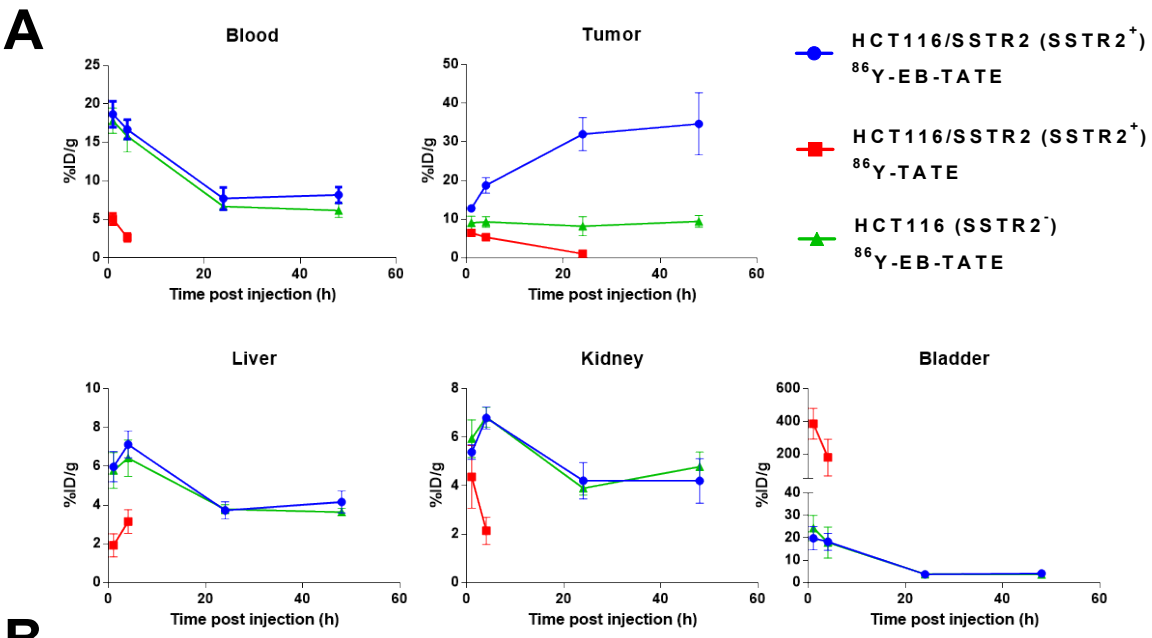
A
Blood
Tumor
Liver
Kidney
Bladder
%ID/g
Time post injection (h)
HCT116/SSTR2 (SSTR2+) 86Y-EB-TATE
HCT116/SSTR2 (SSTR2+) 86Y-TATE
HCT116 (SSTR2-) 86Y-EB-TATE

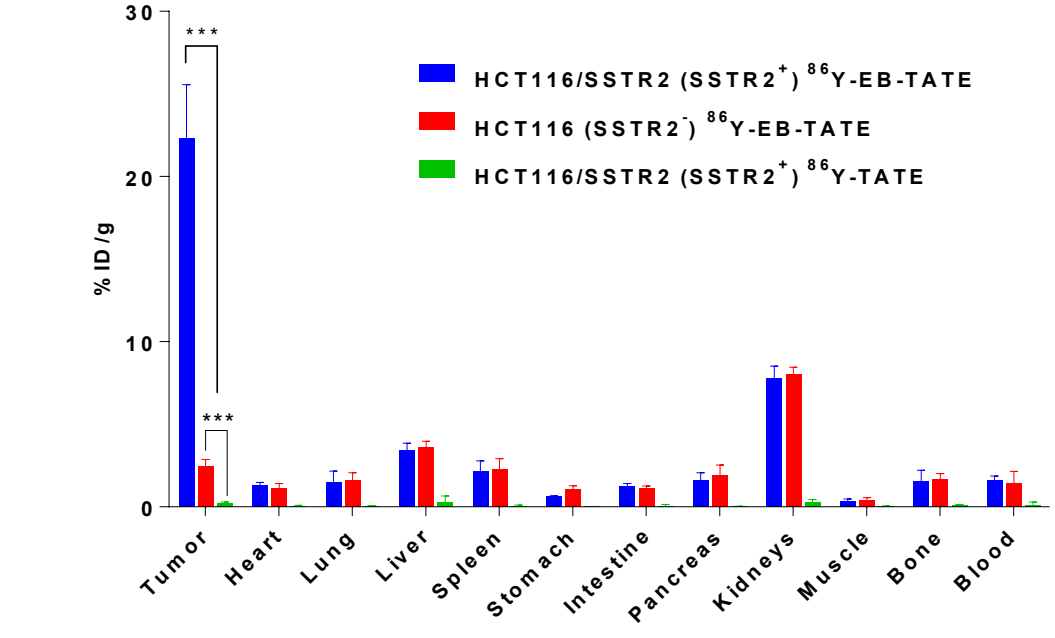
B
% ID/g
***
***
HCT116/SSTR2 (SSTR2+) 86Y-EB-TATE
HCT116 (SSTR2-) 86Y-EB-TATE
HCT116/SSTR2 (SSTR2+) 86Y-TATE
Tumor
Heart
Lung
Liver
Spleen
Stomach
Intestine
Pancreas
Kidneys
Muscle
Bone
Blood

Figure S3

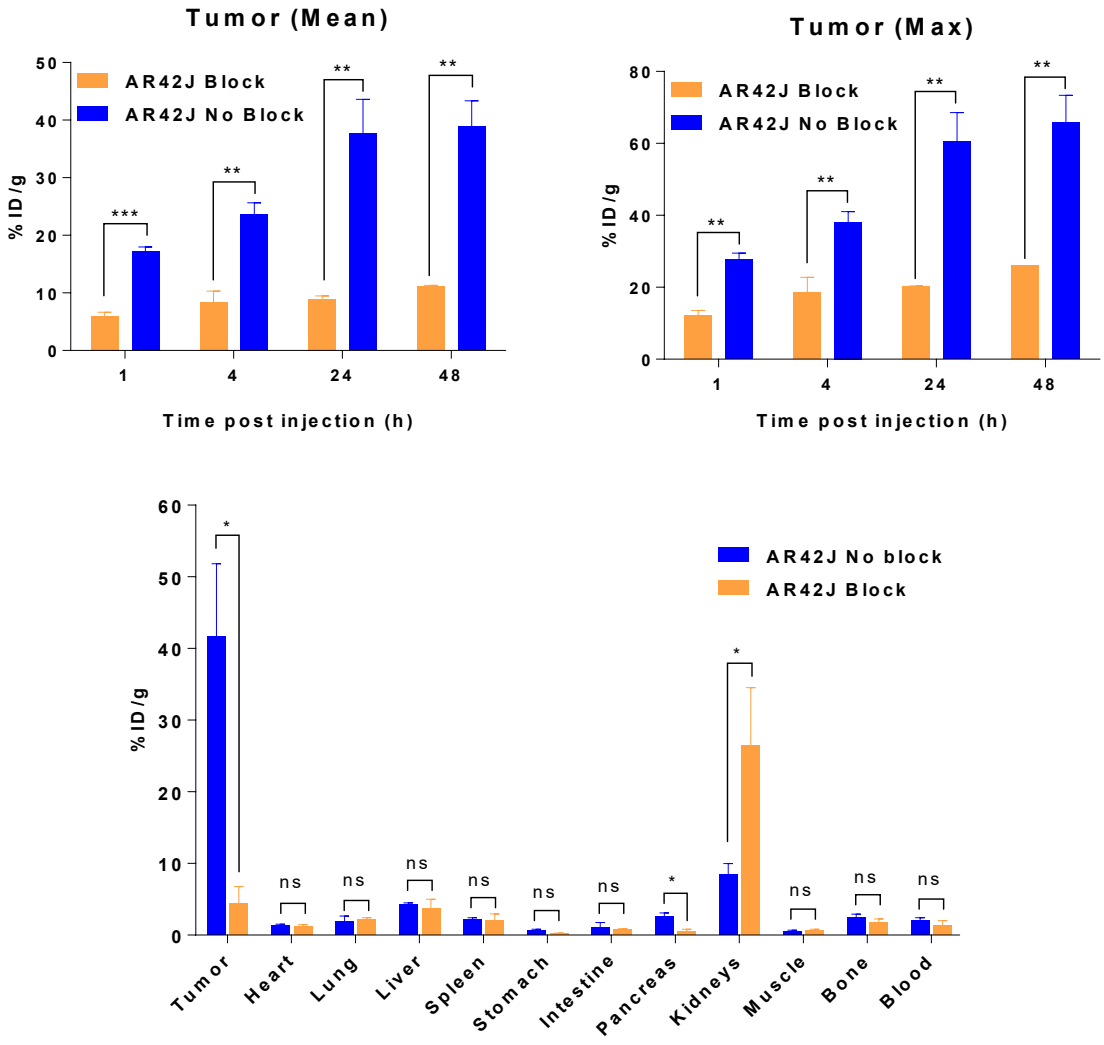
Tumor (Mean)
AR42J Block
AR42J No Block
% ID/g
Time post injection (h)
Tumor (Max)
AR42J Block
AR42J No Block
% ID/g
Time post injection (h)
AR42J No block
AR42J Block
% ID/g
Tumor
Heart
Lung
Liver
Spleen
Stomach
Intestine
Pancreas
Kidneys
Muscle
Bone
Blood

Figure S4

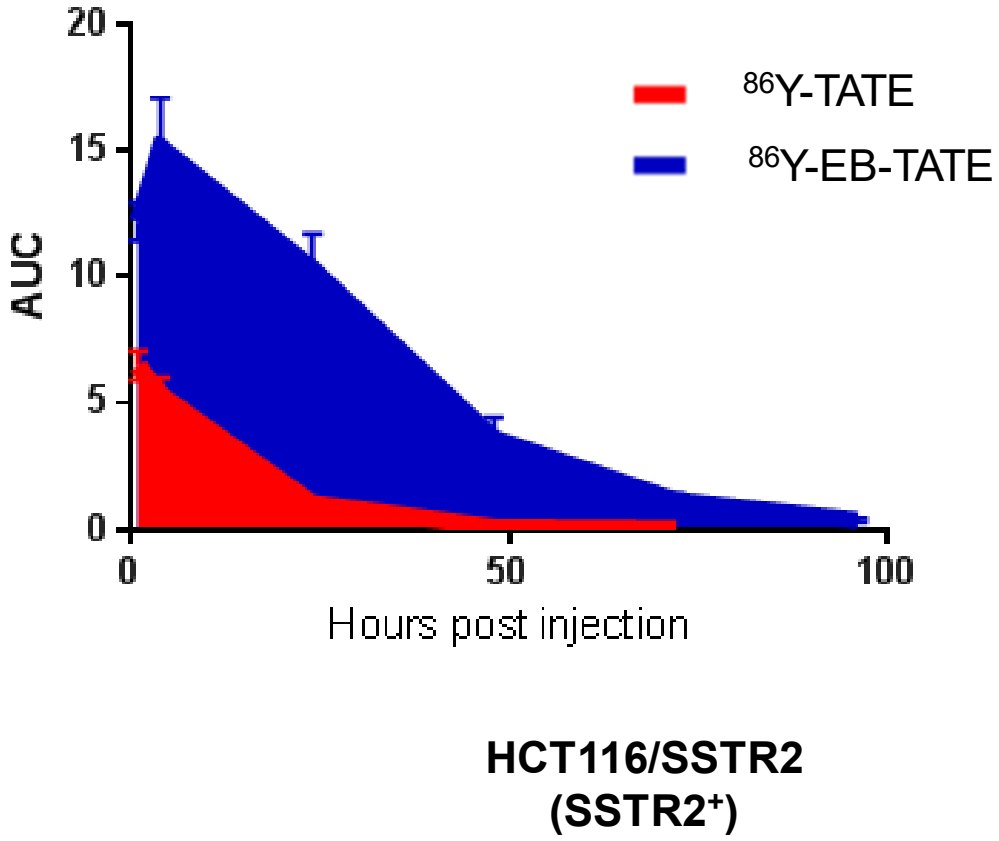
20
15
10
5
0
AUC
0
50
100
Hours post injection
86Y-TATE
86Y-EB-TATE
HCT116/SSTR2
(SSTR2+)

Figure S5

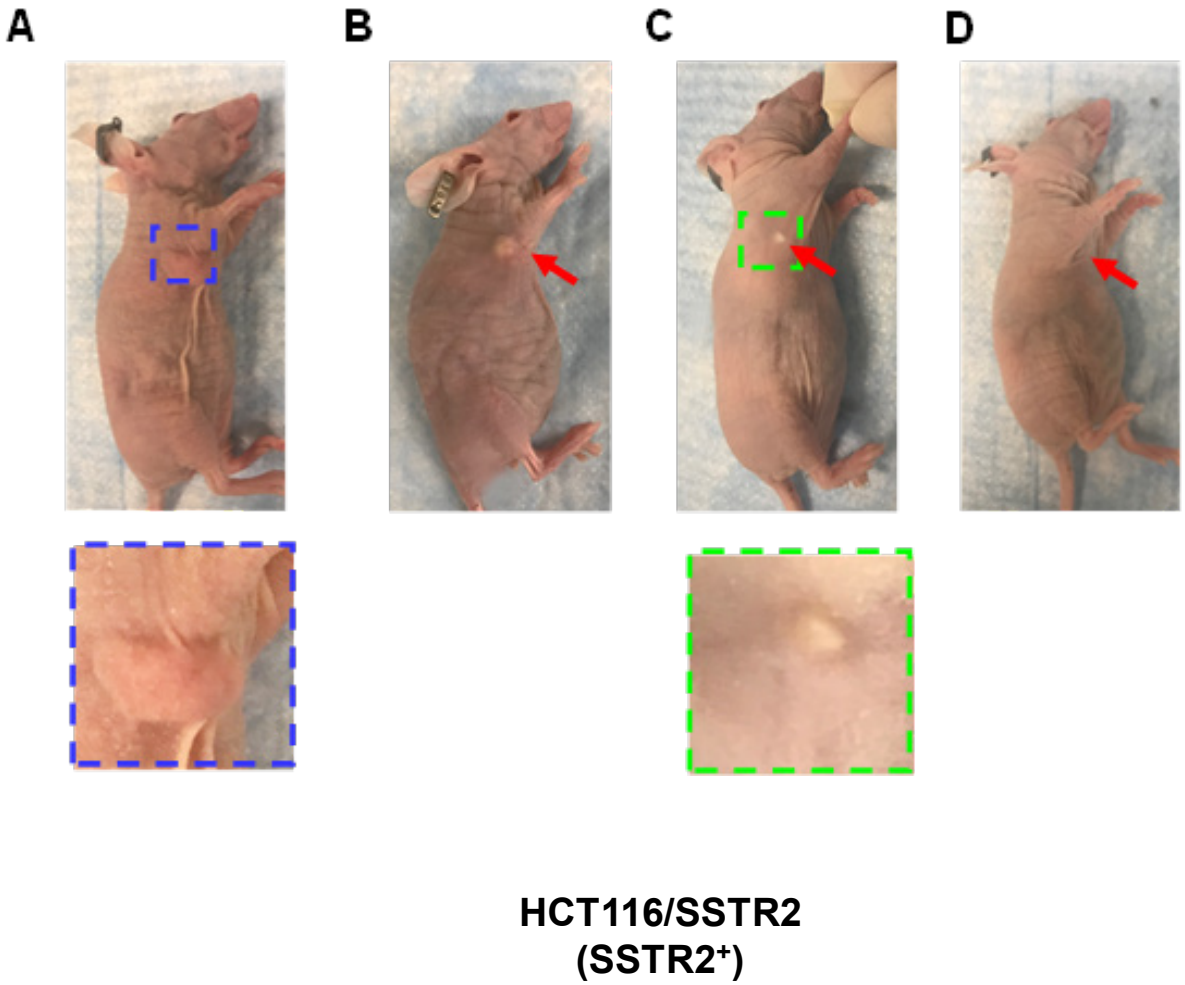

Figure S6

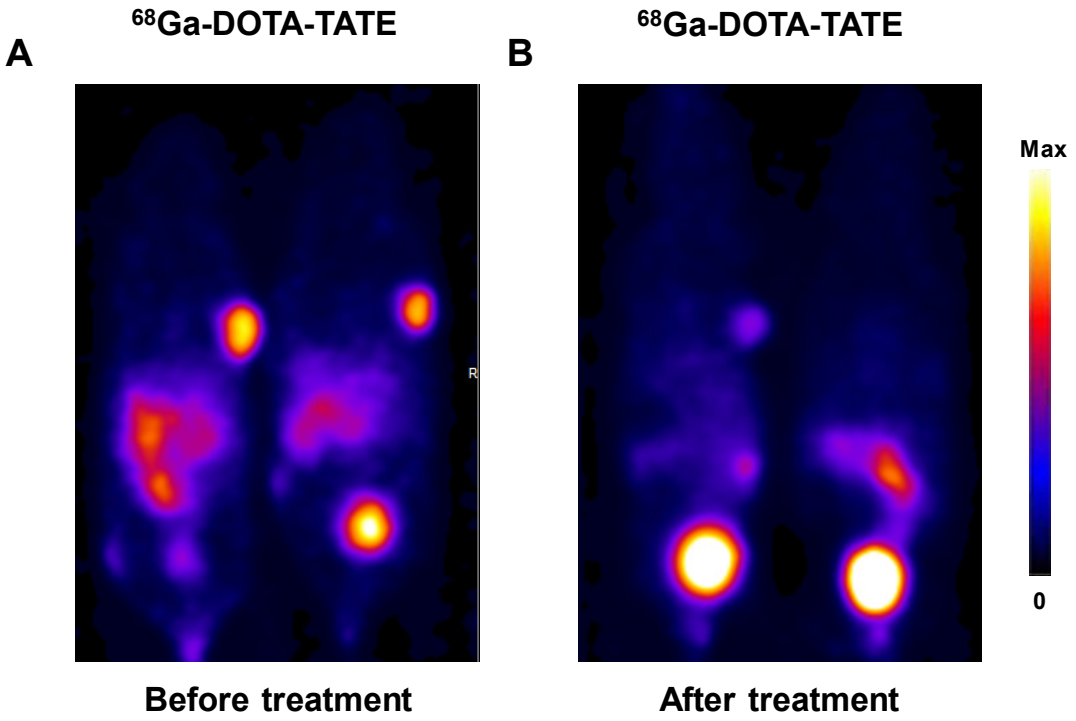
A
68Ga-DOTA-TATE
B
68Ga-DOTA-TATE
Max
0
Before treatment
After treatment
HCT116/SSTR2

Figure S7

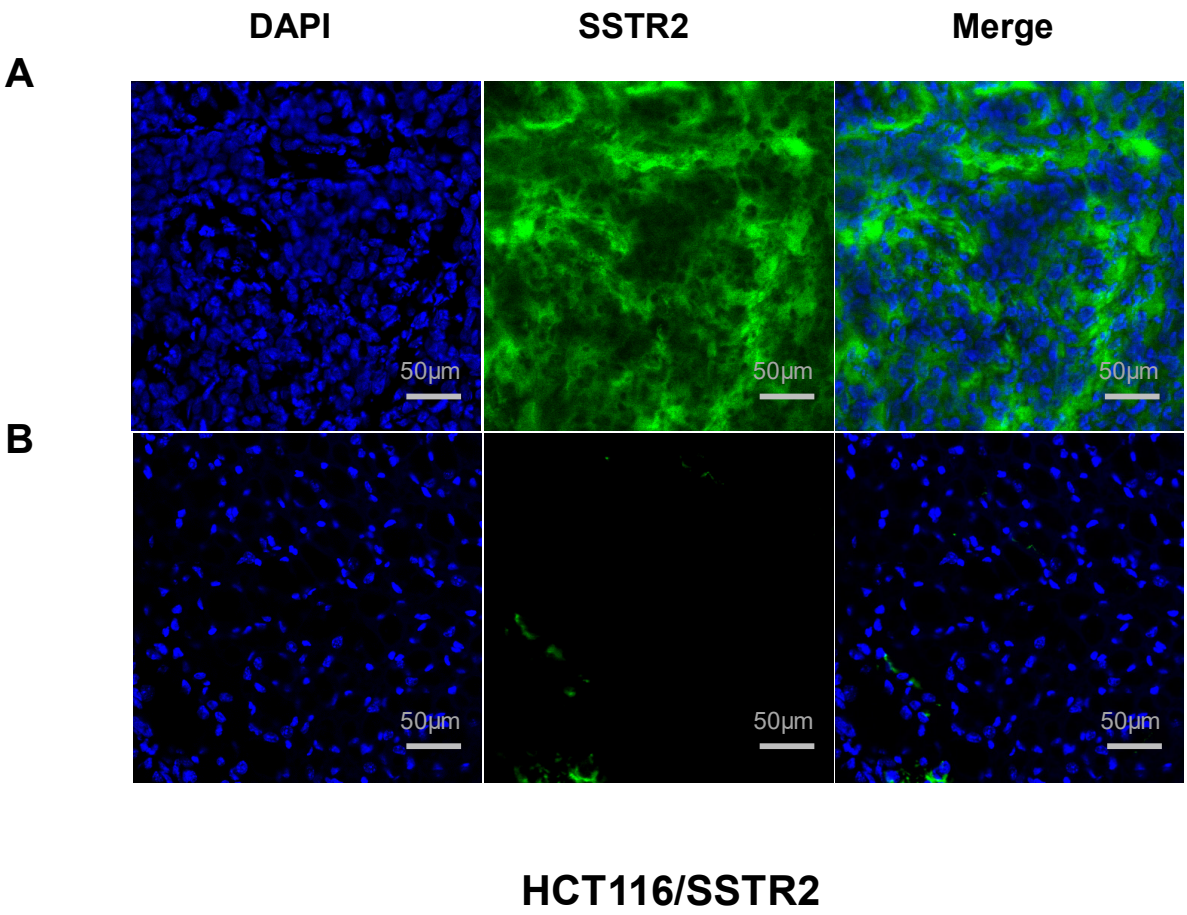
DAPI
SSTR2
Merge
A
B
50μm
50μm
50μm
50μm
50μm
50μm
HCT116/SSTR2

Figure S8

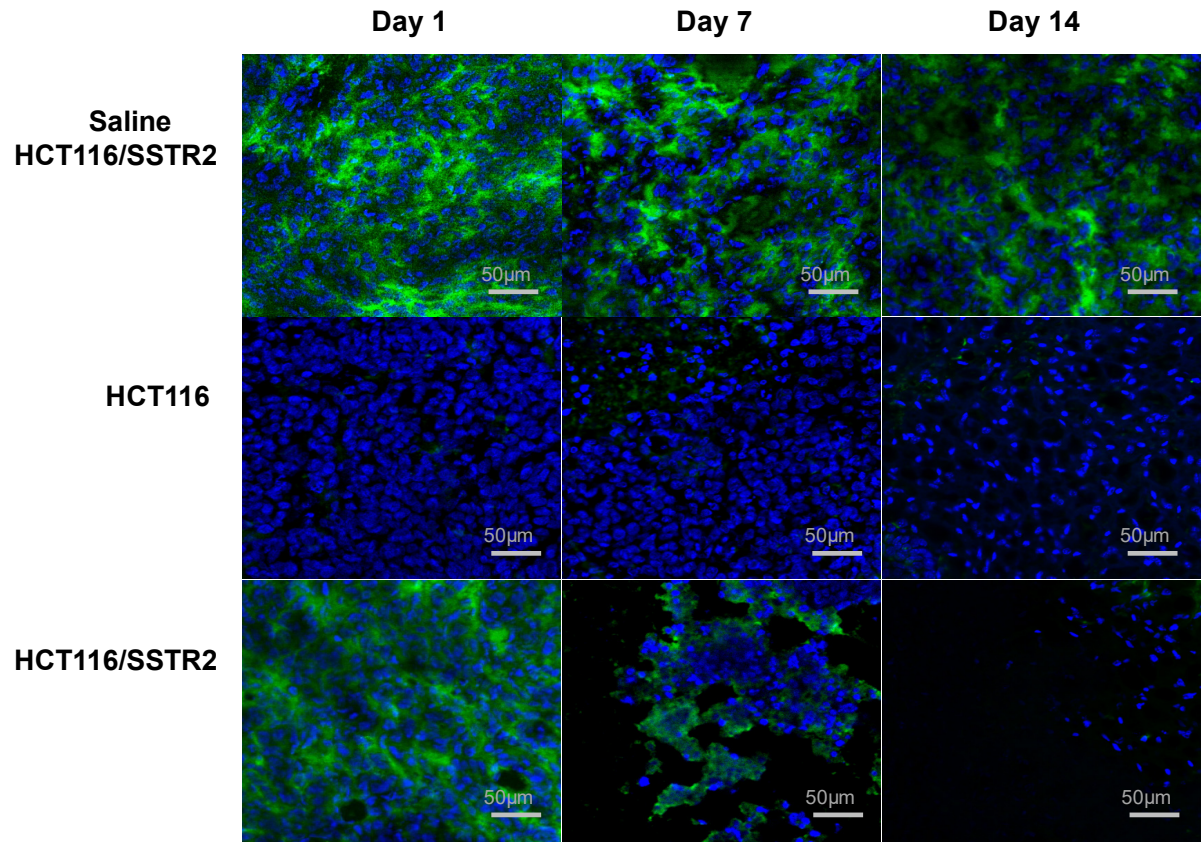
Day 1
Day 7
Day 14
Saline
HCT116/SSTR2
HCT116
HCT116/SSTR2
50μm

Figure S9

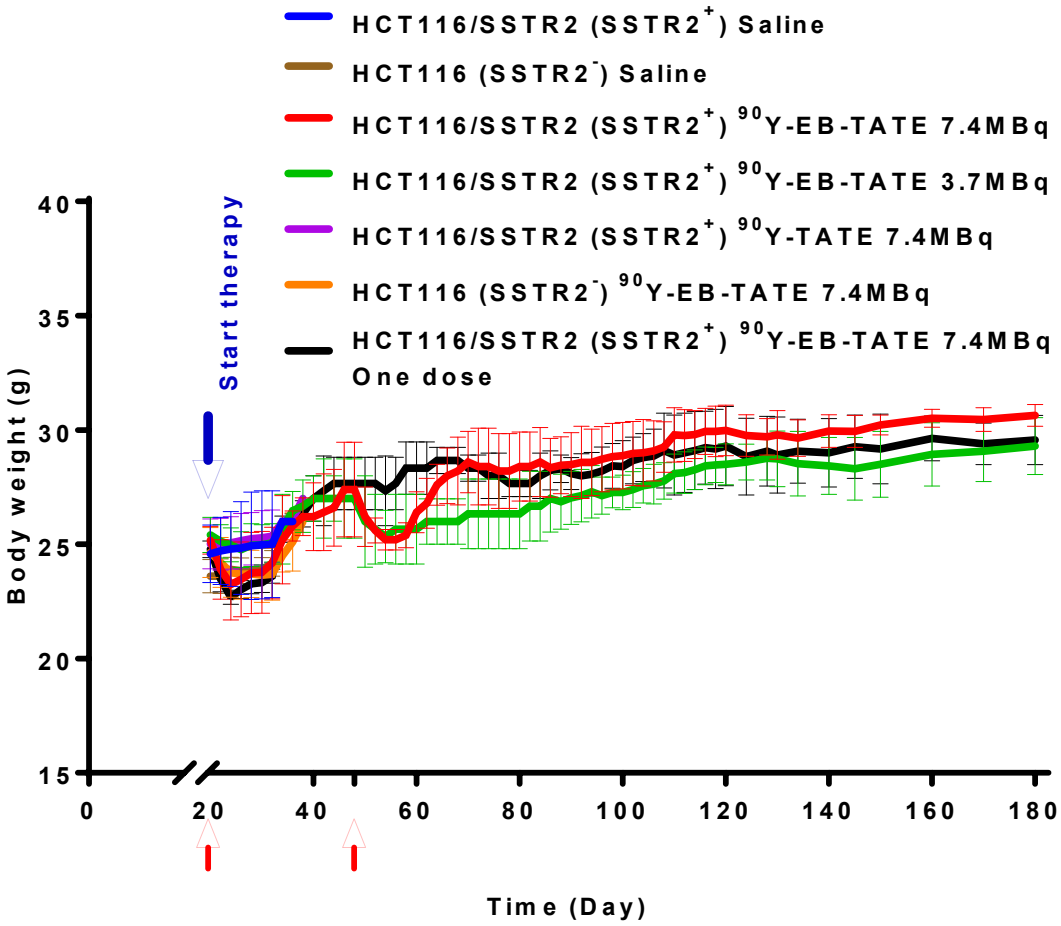
HCT116/SSTR2 (SSTR2+) Saline
HCT116 (SSTR2-) Saline
HCT116/SSTR2 (SSTR2+) 90Y-EB-TATE 7.4MBq
HCT116/SSTR2 (SSTR2+) 90Y-EB-TATE 3.7MBq
HCT116/SSTR2 (SSTR2+) 90Y-TATE 7.4MBq
HCT116 (SSTR2-) 90Y-EB-TATE 7.4MBq
HCT116/SSTR2 (SSTR2+) 90Y-EB-TATE 7.4MBq
One dose
Start therapy
Body weight (g)
40
35
30
25
20
15
0
20
40
60
80
100
120
140
160
180
Time (Day)

Figure S10

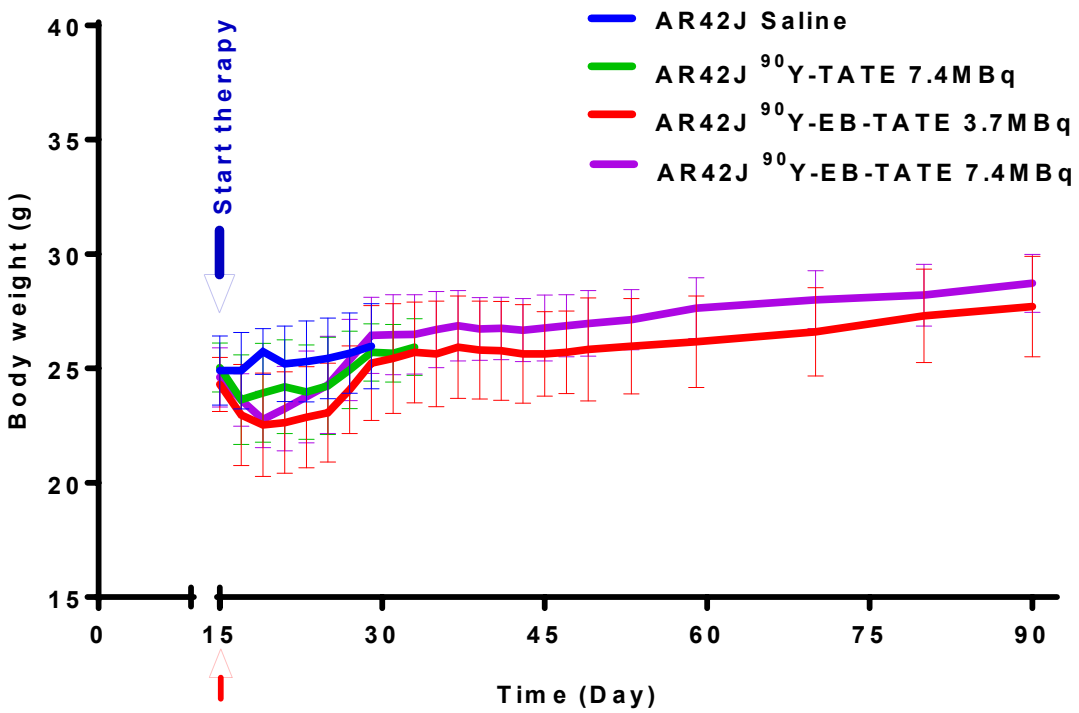
AR42J Saline
AR42J 90Y-TATE 7.4MBq
AR42J 90Y-EB-TATE 3.7MBq
AR42J 90Y-EB-TATE 7.4MBq
Start therapy
Body weight (g)
40
35
30
25
20
15
0
15
30
45
60
75
90
Time (Day)

Figure S11

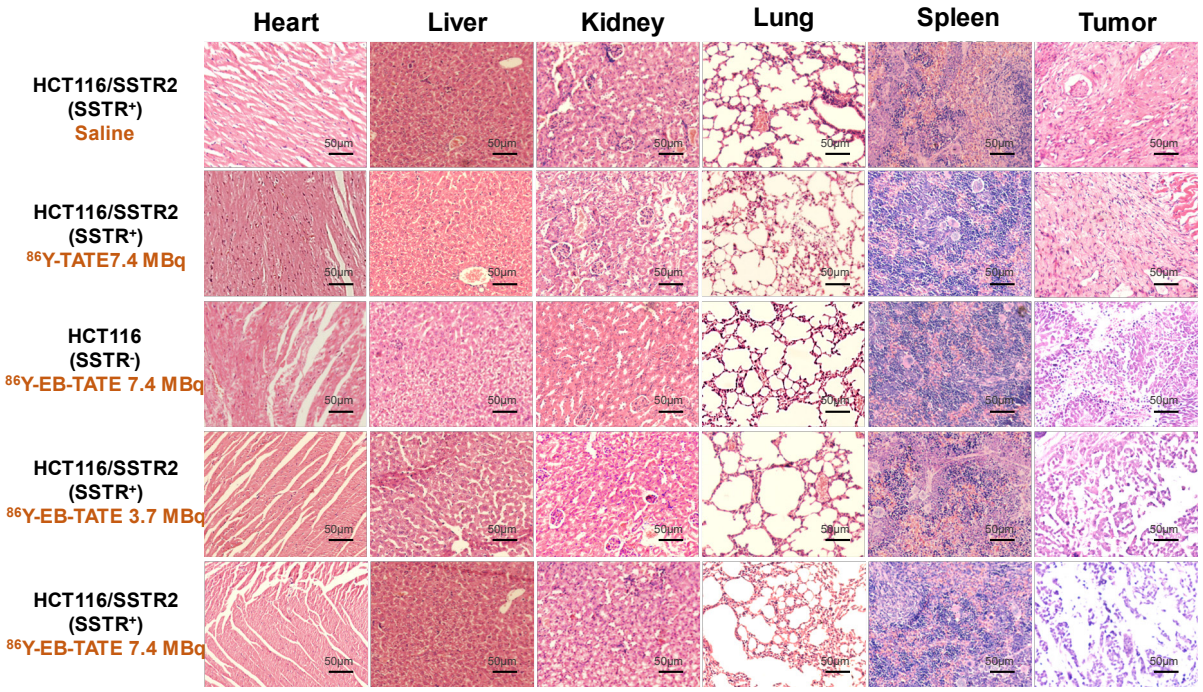
Heart
Liver
Kidney
Lung
Spleen
Tumor
HCT116/SSTR2
(SSTR+)
Saline
HCT116/SSTR2
(SSTR+)
86Y-TATE7.4 MBq
HCT116
(SSTR-)
86Y-EB-TATE 7.4 MBq
HCT116/SSTR2
(SSTR+)
86Y-EB-TATE 3.7 MBq
HCT116/SSTR2
(SSTR+)
86Y-EB-TATE 7.4 MBq
50μm

Figure S12

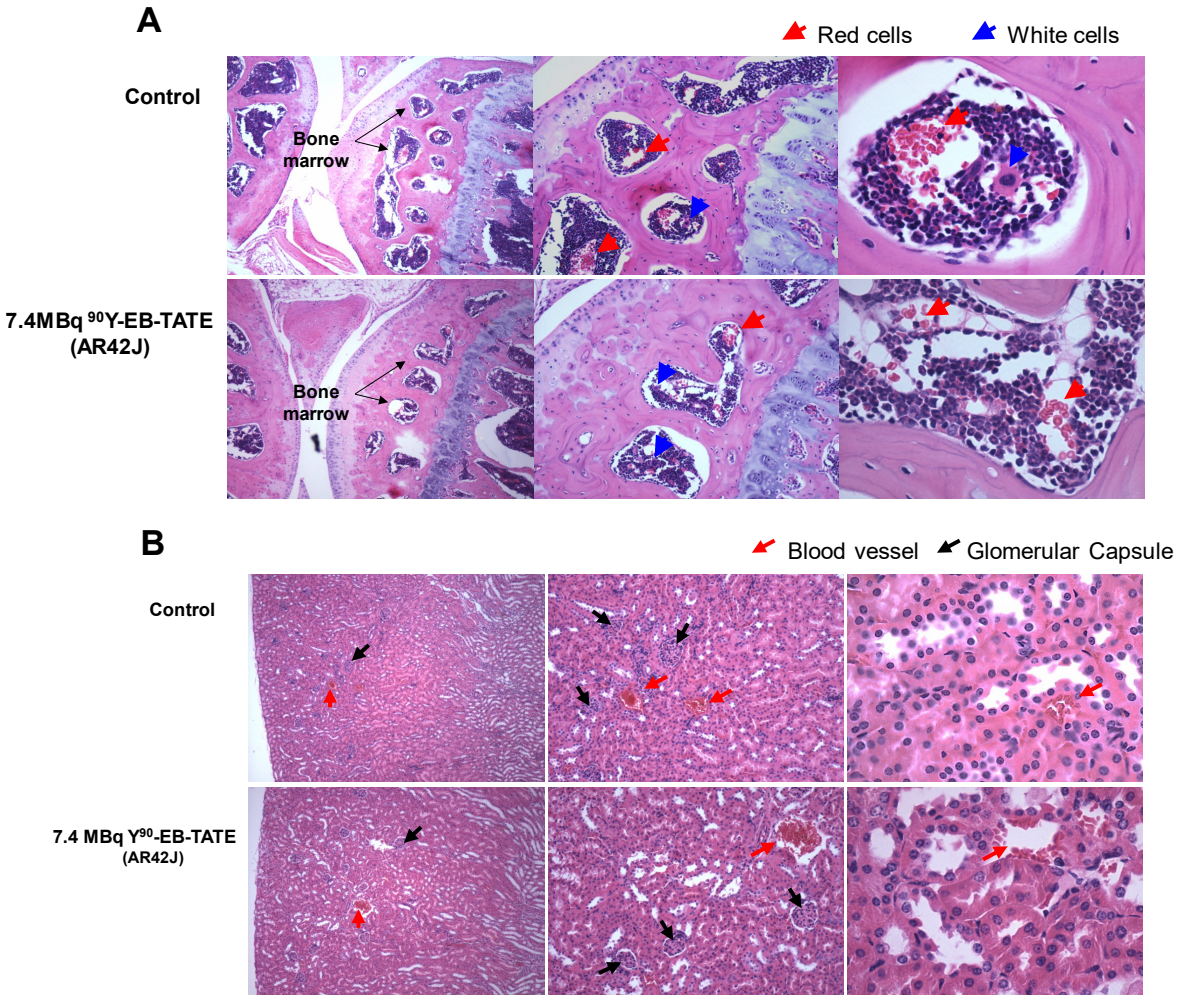
A
Red cells
White cells
Control
Bone marrow
7.4MBq 90Y-EB-TATE (AR42J)
Bone marrow
B
Blood vessel
Glomerular Capsule
Control
7.4 MBq Y90-EB-TATE (AR42J)

Figure S13

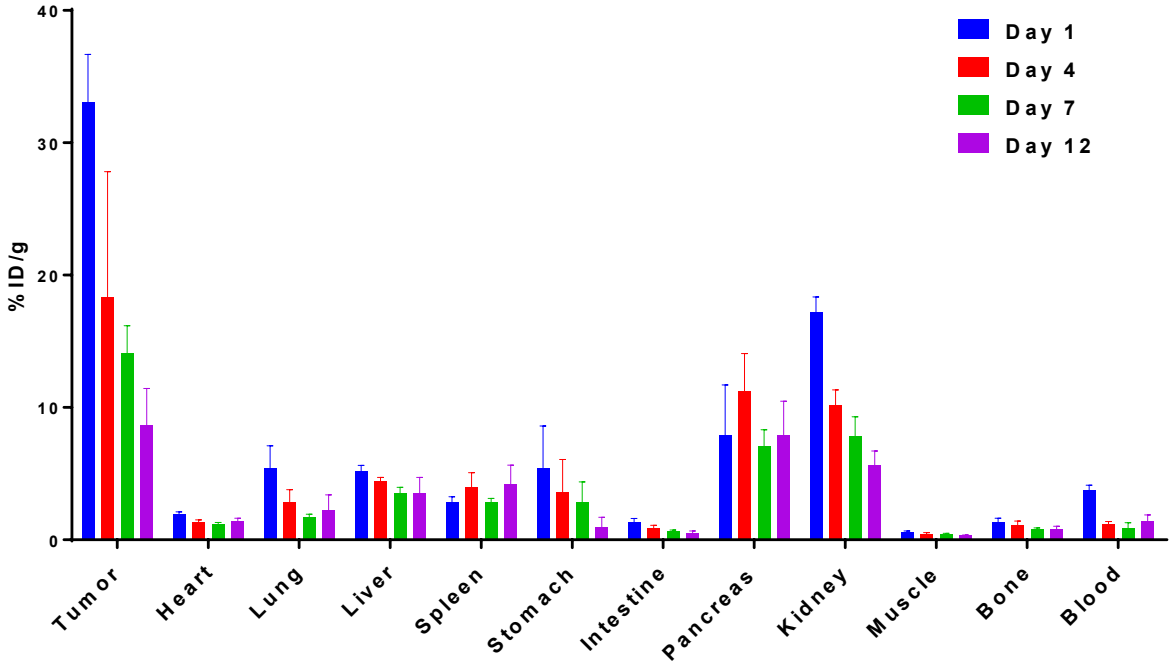
40
30
20
10
0
% ID/g
Day 1
Day 4
Day 7
Day 12
Tumor
Heart
Lung
Liver
Spleen
Stomach
Intestine
Pancreas
Kidney
Muscle
Bone
Blood

Figure S14

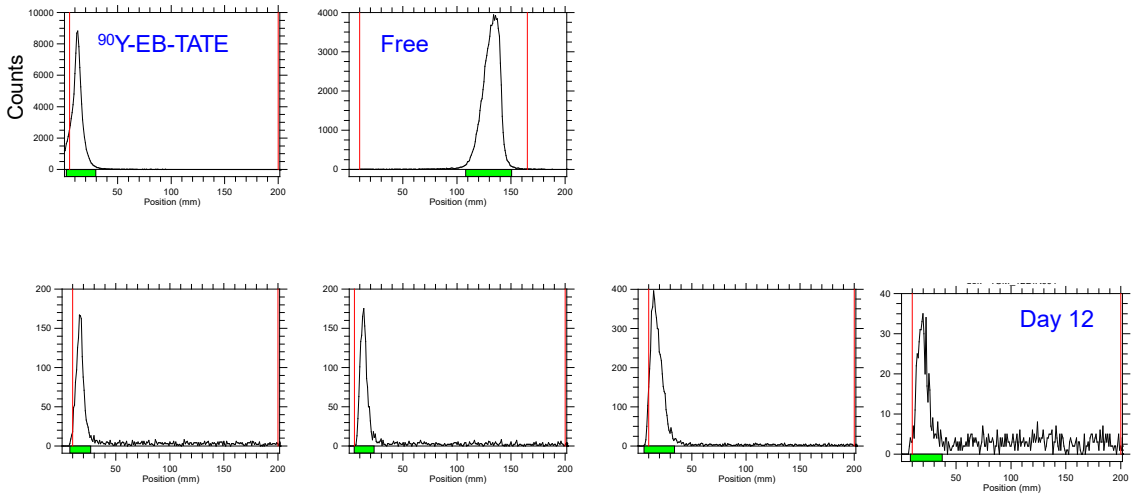

Figure S15

References

1. Chen H, Jacobson O, Niu G*, et al.* Novel "Add-On" Molecule Based on Evans Blue Confers Superior Pharmacokinetics and Transforms Drugs to Theranostic Agents. J Nucl Med 2017;58: 590-7.
2. Chen X, Li L, Liu F, Liu B. Synthesis and biological evaluation of technetium-99m-labeled deoxyglucose derivatives as imaging agents for tumor. Bioorg Med Chem Lett 2006;16: 5503-6.
3. Lang L, Li W, Guo N*, et al.* Comparison study of [^{18}F]FAl-NOTA-PRGD2, [^{18}F]FPPRGD2, and [^{68}Ga]Ga-NOTA-PRGD2 for PET imaging of U87MG tumors in mice. Bioconjug Chem 2011;22: 2415-22.